



CHALMERS
UNIVERSITY OF TECHNOLOGY

A common polar dye additive as corrosion inhibitor and leveling agent for stable aqueous zinc-ion batteries

Downloaded from: <https://research.chalmers.se>, 2025-05-09 08:05 UTC

Citation for the original published paper (version of record):

Wang, H., Hu, C., Yang, Z. et al (2024). A common polar dye additive as corrosion inhibitor and leveling agent for stable aqueous zinc-ion batteries. *Electron*, 2(1). <http://dx.doi.org/10.1002/elt2.21>

N.B. When citing this work, cite the original published paper.

A common polar dye additive as corrosion inhibitor and leveling agent for stable aqueous zinc-ion batteries

Hao Wang¹ | Chao Hu¹ | Zefang Yang¹ | Tingqing Wu¹ | Yihu Li² | Qi Zhang¹ | Yougen Tang¹ | Haiyan Wang¹ 

¹Hunan Provincial Key Laboratory of Chemical Power Sources, College of Chemistry and Chemical Engineering, Central South University, Changsha, China

²Department of Physics, Chalmers University of Technology, Gothenburg, Sweden

Correspondence

Qi Zhang and Haiyan Wang.
Email: qzhang1027@csu.edu.cn and wanghy419@csu.edu.cn

Funding information

National Natural Science Foundation of China, Grant/Award Numbers: 21975289, 22109181; Hunan Provincial Science and Technology Plan Projects of China, Grant/Award Numbers: 2017TP1001, 2020JJ2042, 2022RC3050; Hunan Provincial Natural Science Foundation of China, Grant/Award Number: 2022JJ40576; Fundamental Research Funds for the Central Universities Central South University, Grant/Award Number: 2023ZZTS0511

Abstract

The industrial application of zinc-ion batteries is restricted by irrepressible dendrite growth and side reactions that resulted from the surface heterogeneity of the commercial zinc electrode and the thermodynamic spontaneous corrosion in a weakly acidic aqueous electrolyte. Herein, a common polar dye, Procion Red MX-5b, with high polarity and asymmetric charge distribution is introduced into the zinc sulfate electrolyte, which can not only reconstruct the solvation configuration of Zn²⁺ and strengthen hydrogen bonding to reduce the reactivity of free H₂O but also homogenize interfacial electric field by its preferentially absorption on the zinc surface. The symmetric cell can cycle with a lower voltage hysteresis (78.4 mV) for 1120 times at 5 mA cm⁻² and Zn//NaV₃O₈·1.5H₂O full cell can be cycled over 1000 times with high capacity (average 170 mAh g⁻¹) at 4 A g⁻¹ in the compound electrolyte. This study provides a new perspective for additive engineering strategies of aqueous zinc-ion batteries.

KEYWORDS

corrosion inhibitor, leveling agent, multifunctional additive, solvation structure, zinc-ion batteries

1 | INTRODUCTION

The natural advantages of high energy density and long cycle life have established dominant position of lithium-ion batteries in the energy storage market.¹⁻³ Despite these remarkable features, their further development has been hampered by limited lithium reserves, rising raw material costs and safety concerns arising from combustible organic electrolytes.⁴ Aqueous zinc-ion batteries (AZIBs) are conspicuous due to high natural abundance, safety and high

theoretical capacity (820 mAh g⁻¹).⁵ However, side reactions at electrode–electrolyte interface (EEI) can induce electrolyte loss and impedance increase and the uncontrolled and rampant dendrite growth during charge–discharge cycles can potentially result in internal short circuits, severely limiting the commercialization process of AZIBs.⁶

Numerous strategies, such as current collector design,^{7,8} zinc metal modification,⁹⁻¹² separator optimization,^{13,14} and electrolyte engineering,^{15,16} can address these above issues. Among them, the

Hao Wang and Chao Hu contributed to this work equally.

This is an open access article under the terms of the [Creative Commons Attribution](https://creativecommons.org/licenses/by/4.0/) License, which permits use, distribution and reproduction in any medium, provided the original work is properly cited.

© 2023 The Authors. *Electron* published by Harbin Institute of Technology and John Wiley & Sons Australia, Ltd.

introduction of functional additives is an effective method because of its simplicity and scalability. Some highly polar organic molecules (e.g., methanol,¹⁷ glucose,¹⁸ dimethyl sulfoxide,¹⁹ and N-methylpyrrolidone²⁰) can reconstruct the solvent sheath of Zn^{2+} by their strong interaction with Zn^{2+} in aqueous electrolyte. This results in a decrease in the amount of bound H_2O and the activity of free H_2O , which effectively inhibit the side reaction between zinc and H_2O . Some other additives (e.g., polyacrylamide,²¹ thiourea,²² and cysteine²³) can be used as corrosion inhibitors for zinc anode, which preferentially form a hydrophobic protective layer that reduces the rate of zinc corrosion. In addition, many mechanisms have been proposed to resolve the optimized interfacial reactions under the effect of additives. For example, the electrostatic shielding effect of cationic additives²⁴ was used to reveal the reaction mechanism of progressive nucleation,²⁵ and the highly charged cations can compress the interface electric double layers to achieve uniform zinc deposition.²⁶ The anionic coordination can reform the inner Helmholtz layer and specify the orientation of crystal surface.^{27–29} However, the evolution at EEI during electrochemical zinc stripping/plating remains unclear. Therefore, it is necessary to develop an inexpensive multifunctional additive suitable for AZIBs and deeply analyze its dynamic mechanism.

Herein, a common polar dye, Procion Red MX-5b (PR), was selected as a comprehensive electrolyte additive for highly reversible AZIBs. The theoretical calculations and experiments indicate that PR can strengthen the H-bond network by its numerous polar sites and reconstruct solvation configuration of Zn^{2+} to weaken the activity of H_2O in the electrolyte, thus inhibiting side reactions and improving the stability of the zinc anode. Based on the dynamic observation of zinc stripping/plating behavior, it was found that PR adsorption modifies the surface electric field, which eliminates the preference of crystal orientation of zinc stripping/plating and significantly improves the life span of AZIBs (Table S1).

2 | RESULTS AND DISCUSSION

The electrode surface is generally electronegative, that is, attracting cations and repelling anions.²⁸ However, the electronegativity of the electrode interface may be adjusted when the anion characteristic adsorption effect is stronger than electrostatic repulsion or anionic characteristic groups can be combined with the electrode surface.²⁹ Three polar molecules were evaluated for their potential as electrolyte additives of AZIBs, including PR, Reactive Red

24 (RR), and methyl orange (MO), which all can dissociate into anions. These high polarized molecules can interact strongly with H_2O and Zn^{2+} by their $-\text{SO}_3^-$ or deprotonated hydroxyl groups. PR shows higher electronegativity than MO according to the calculated electrostatic potential and the weaker spatial effect of PR compared to RR facilitates its interaction with cations and H_2O (Figure 1A and Figure S1), which indicates that PR is preferred for electrolyte engineering design because of its high polarity, great adsorption, and strong affinity with charged metal ions.³⁰ It is also confirmed in the preliminary experiment that the introduction of PR can reduce the impedance of electrolyte and inhibit

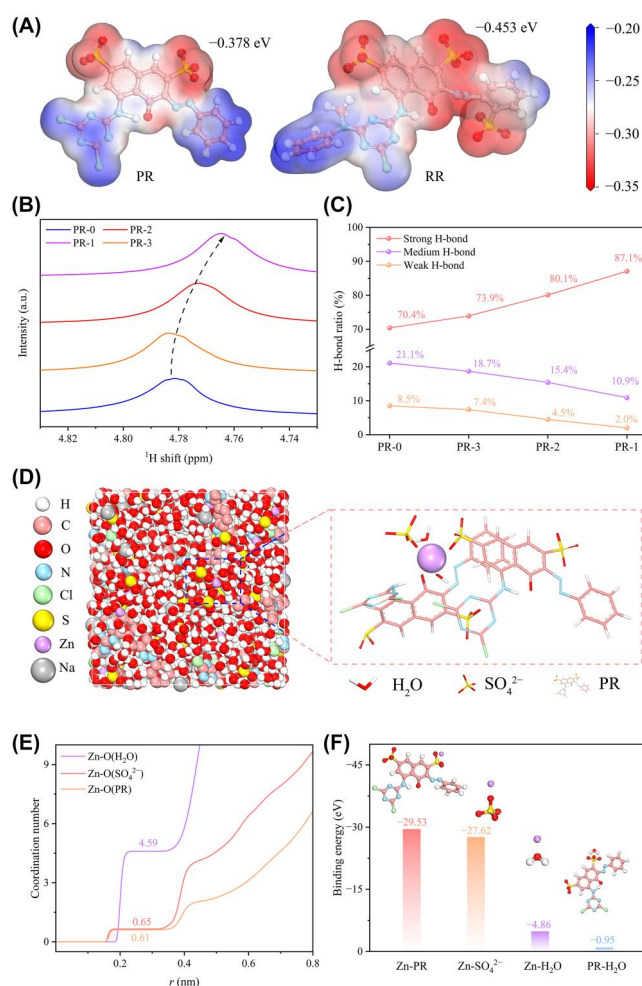


FIGURE 1 (A) Electrostatic potential mappings of PR and RR. (B) ^1H spectra of different electrolytes. (C) Ratio of strong, medium, and weak H-bonds in different electrolytes. (D) Snapshot of PR-2 electrolyte in MD simulations and solvated structure in local magnification view. (E) CN of Zn-O in the electrolyte with PR. (F) Calculated binding energy between different molecules (Zn^{2+} , SO_4^{2-} , PR, H_2O) by DFT calculation. CN, coordination number; DFT, density functional theory; MD, molecular dynamics; PR, Procion Red MX-5b; RR, Reactive Red 24.

zinc corrosion (Figure S2), increasing the life span of symmetric cells (Figure S3). Therefore, PR is chosen as the optimum high polarized molecule to explore the impact of anions on electrolytes. A series of composite electrolytes were prepared with different concentrations of PR (10^{-x} g L⁻¹, denoted as PR-X, X = 1, 2, 3) in 2 mol L⁻¹ ZnSO₄ electrolytes (PR-0). With increasing PR concentration, the electrolytes gradually turn deep red but remain transparent (Figure S4), which indicates that the electrolyte remains stable after the interaction between PR and Zn²⁺.³¹ As shown in the conductivity measurement (Figure S5), the small amount of PR contributes to Zn²⁺ migration, but the conductivity decreases when its content increases, which may be attributed to the repulsion effect of Na⁺ and steric hindrance of PR.³² The results of Fourier transform infrared spectra and nuclear magnetic resonance investigate and verify the interaction of different molecules. With increasing PR concentration, the blue-shifted stretching vibration of SO₄²⁻ from 1077.8 cm⁻¹ to 1088.4 cm⁻¹ (Figure S6) suggests that PR reconstructs solvation configuration and involves SO₄²⁻ in the first shell that interacts directly with Zn²⁺.¹⁷ The ¹H peak (Figure 1B) exhibits a slight increase followed by a significant decrease, which might attribute to different influence between hydrogen bonding of H₂O and high electron density of PR on the shielding effect.³³ O-H peaks (2900–3800 cm⁻¹) can be divided into three types of H-bonds (Figure S7).³⁴ In detail, the proportion of strong H-bond at PR-1 increases significantly to 87.1%, while the medium and weak H-bond gradually decreases from 21.1% to 10.9% and from 8.5% to 2.0%, respectively (Figure 1C), indicating that PR can destroy Zn²⁺ solvation configuration, release bound H₂O, and the strengthen H-bond network.³⁵

The solvation configuration in different electrolytes were further confirmed by molecular dynamics (MD) simulations and density functional theory calculations. The trivalent anion of PR was applied for simulations and calculations because PR can be deprotonated, as evidenced by the pH decrease of the electrolyte (Figure S8).³³ The MD simulation of the electrolyte without PR (Figure S9) reveals that the first solvent sheath is formed by the coordination of Zn²⁺ with six H₂O molecules or five H₂O molecules and SO₄²⁻. In comparison, several new solvation structures composed of H₂O, SO₄²⁻, and PR (Figure 1D and Figure S10) were observed in the electrolyte with PR. The radial distribution functions and coordination numbers (CNs) of different electrolytes were analyzed to quantitatively characterize the solvation configuration. In additive-free electrolyte, the peaks of Zn-O at 0.201 nm and 0.163 nm

were derived from H₂O and SO₄²⁻ (Figure S11a). In contrast, a new peak appears at 0.169 nm in the electrolyte with PR (Figure S11b), suggesting that some PR are involved in the construction of the first shell. Besides, the CNs of Zn²⁺ in the first solvent sheath using the electrolyte without PR are 5.76 (Zn-H₂O) and 0.40 (Zn-SO₄²⁻), while the CNs of Zn-H₂O, Zn-SO₄²⁻, and Zn-PR after adding PR are 4.59, 0.65, and 0.61, respectively (Figure 1E and Figure S12). These results indicate that PR can cooperate with SO₄²⁻ to reconstruct the solvent sheath resulting in a decrease in the coordinated H₂O of Zn²⁺.³¹ The interaction energies between Zn²⁺, H₂O, SO₄²⁻, PR are calculated and shown in Figure 1F. The binding energies between Zn²⁺ and anions (SO₄²⁻, PR) are significantly higher than that of Zn-H₂O, and the three are much higher than that of H₂O-PR, indicating that Zn²⁺ tends to coordinate with PR and SO₄²⁻, but is limited by steric hindrance and eventually co-builds the first solvent sheath with H₂O.¹⁸ Besides, the binding energies of different interaction models of H₂O, PR, and SO₄²⁻ are much higher than that of H₂O-H₂O, implying that PR can attract H₂O molecules, enhance hydrogen bonding, and reduce activity of free H₂O (Figure S13).

The adsorption energies of different crystal planes and different molecules were calculated to study the adsorption competition between PR and H₂O and the change of interface reaction environment (Figure S14). Obviously, the adsorption energy between Zn and PR is much higher than that of others (Zn-H₂O, -0.23 eV and -0.30 eV), regardless of whether PR is in parallel (-7.79 eV and -7.64 eV) or vertical (-7.48 eV and -7.62 eV) state on any crystal plane of zinc foil (Figure 2A and Figure S15). It can be inferred that PR may adsorb on the zinc foil to form a hydrophobic molecular layer to inhibit zinc corrosion by a weakly acidic electrolyte and dissolved oxygen. As shown in the results of Tafel fitting and numerical analysis (Figure S16 and Figure 2B), it is found that the introduction of PR promotes a slight positive shift of corrosion potential and significant decline of corrosion current, which indicates the formation of protective layer and confirms the specific adsorption effect of PR. In addition, higher hydrogen evolution overpotentials (Figure 2C) of zinc in different electrolytes also prove that PR inhibits corrosion and hydrogen evolution.²¹ Obviously, PR-2 electrolyte has more excellent comprehensive properties. To verify the effect of PR on zinc foil in practical application situation, as compared in Figure S17, zinc foil soaked in pure electrolyte (Zn@PR-0) for 15 days is corroded with serious pits and cracks, while the zinc foil soaked in

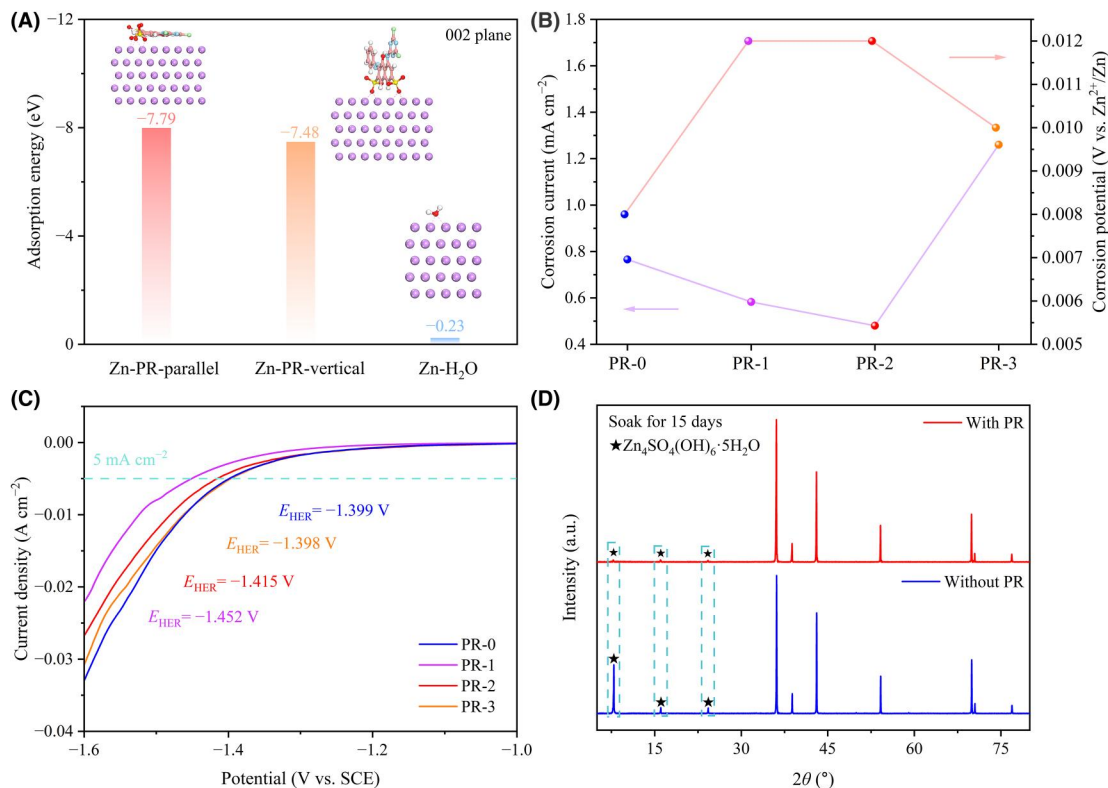


FIGURE 2 (A) Adsorption energy of different combinations, insets show the adsorbed models at side view. (B) Corrosion currents and potentials of Zn in different electrolytes. (C) Linear scan voltammetry curves in different electrolytes at 1 mV s⁻¹. (D) XRD of zinc foil after immersion for 15 days in different electrolytes. HER, hydrogen evolution reaction; PR, Procion Red MX-5b; SCE, saturated calomel electrode; XRD, X-ray diffraction.

compound electrolyte (Zn@PR-2) shows corrosion traces only in some parts.²² The negligible by-product characteristic peaks in X-ray diffraction (XRD) spectra of Zn@PR-2 confirm the difference of morphology (Figure 2D).

Based on in situ optical microscope observations (Figure S18), zinc is preferentially reduced at highly active sites and evolves into rampant dendrites in the electrolyte without PR. However, PR adsorbed in the weak electric field induces in situ deposition of zinc to fill the depression and diffuse to the surrounding area to achieve a macroscopic uniform morphology. As shown in Figure S19, PR protective layer cannot completely cover the surface of zinc foil in PR-3 electrolyte which can reduce the holes but cannot change uneven stripping behavior, while large volume of anions and sodium ions compete with each other in PR-1 electrolyte, resulting in uniform stripping with local pores. Zinc foil remained flat only after stripping for 1 mAh cm⁻² in PR-2 electrolyte in contrast to the obvious cavities in the PR-0 electrolyte. Similar zinc stripping behavior trends are shown in different electrolytes, respectively (Figure 3A–D), even if the stripping capacity is increased to 2 mAh

cm⁻². PR adsorption can passivate the depression on the zinc surface and facilitate the preferential stripping of protruding part with high activity. The resultant flat zinc surface is conducive to the subsequent zinc deposition.³⁶ Furthermore, the morphologies and crystallographic characteristics of zinc foil after 20 cycles were examined to determine the effect of PR on the electrochemical cycling process. In detail, zinc nucleates at some dispersed active nucleation sites in PR-0 electrolyte, forming uneven massive dendrites and by-products (Figure 3E). The massive zinc dendrites disappear but there are still obvious voids and loose sheet by-products (Figure 3F) in PR-3 electrolyte. On the contrary, zinc foil in the electrolyte with PR becomes dense and uniform from loose flower-like deposition (Figure 3G), which is more conducive to the denser zinc deposition by the homogenized electric field and reduced difference in interfacial activity. Also, the pores, compact dendrites, and inert flat regions (Figure 3H) in PR-1 electrolyte are the result of repulsive interaction of excessive anions.³⁶ XRD analysis reveals distinct characteristics of zinc foil cycling in PR-0 and PR-3 electrolytes with an obvious peak corresponding to

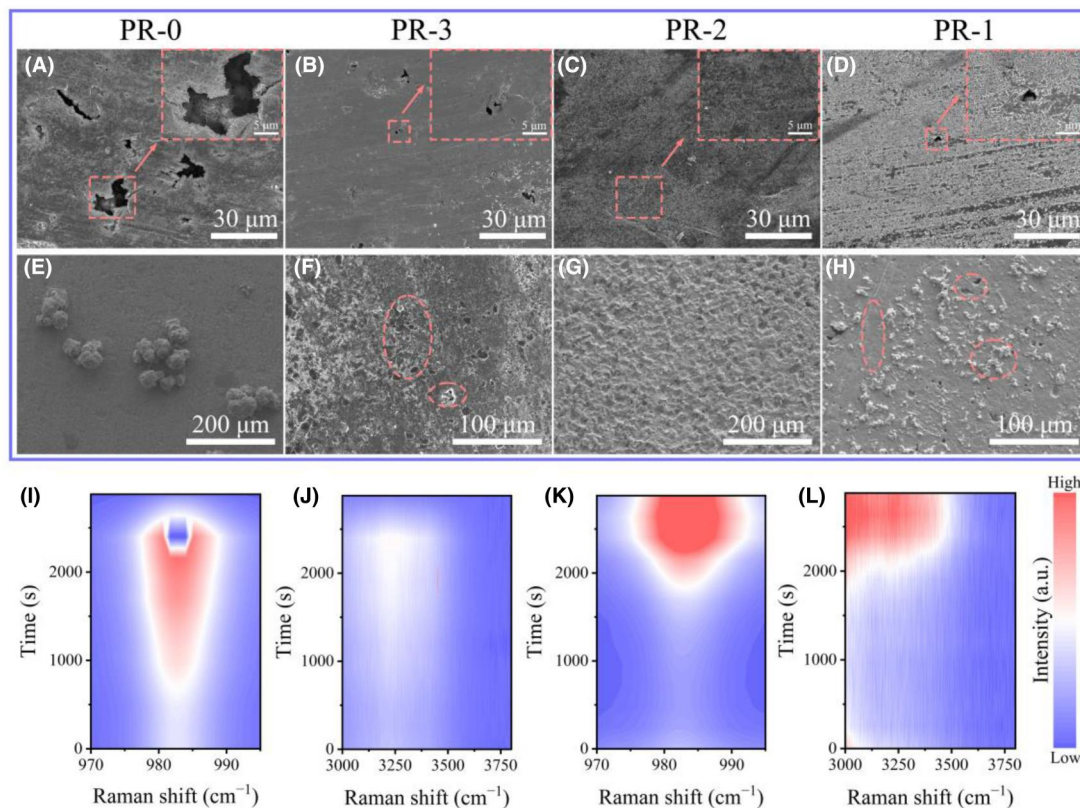


FIGURE 3 (A–D) SEM images of zinc foil after stripping for 2 mAh cm^{-2} in different electrolytes at 5 mA cm^{-2} . (E–H) SEM images of zinc foil after 20 cycles in different electrolytes. In situ Raman spectra of the electrolyte (I, J) without or (K, L) with PR at zinc electrode interface during discharge. PR, Procion Red MX-5b; SEM, scanning electron microscope.

the by-product. In contrast, zinc foil in PR-1 and PR-2 electrolytes retained its pure zinc crystal phase without side effects (Figure S20).

The in situ Raman spectroscopy characterization was applied in exploring dynamic evolution of the adsorption behavior of PR at EEI.³⁷ According to Figure 3I, the peak intensity at 983 cm^{-1} suggests gradual increase of SO_4^{2-} concentration during the programmed discharge, which can be attributed to the electrostatic equilibrium formed by the attraction of abundant Zn^{2+} to SO_4^{2-} .³⁸ Similarly, the slightly enhanced and red-shifted H-O peaks at 2900 cm^{-1} – 3800 cm^{-1} (Figure 3J), indicate the enhanced hydrogen bonding owing to the de-solvation of Zn^{2+} .³⁹ In contrast, the characteristic peaks of SO_4^{2-} show more obvious enhancement and red shift in the PR electrolyte (Figure 3K), which may be because of the increased local concentration of SO_4^{2-} resulting from Zn^{2+} de-solvation and the enhanced S-O stretching vibration by the removal of zinc.⁴⁰ Meanwhile, similar changes in H-O bonds are also observed, indicating significant enhancement of local hydrogen bonding (Figure 3L), which may be attrib-

uted to the synergistic effect of PR adsorbed at EEI and SO_4^{2-} on the periphery to reconstruct the H-bond network.⁴¹

Figure 4A shows the hysteresis voltage of zinc symmetric cells in different electrolytes at 5 mA cm^{-2} for 1 mAh cm^{-2} . The cell fails rapidly after 156 cycles (66 h) in the PR-0 electrolyte. However, PR can significantly improve cycling performance with the best performance of 1120 cycles (450 h) in PR-2 electrolyte. The local magnification of the voltage curves shows that PR can reduce polarization and stabilize the plateau potential.⁴² The lowest impedance of symmetric cells with PR-2 electrolyte also proves its excellent performance (Figure S21). In the compound electrolyte, the initial zinc nucleation overpotential is 60.2 mV , lower than that in the pure electrolyte (85.7 mV) (Figure 4B). This lower nucleation barrier indicates the diminished influence of surface activity on the initial nucleation and reduced cycling energy consumption.⁴² Zn//Cu asymmetric cell still exhibits excellent reversibility after 550 cycles at 5 mA cm^{-2} for 1 mAh cm^{-2} with a high Coulombic efficiency

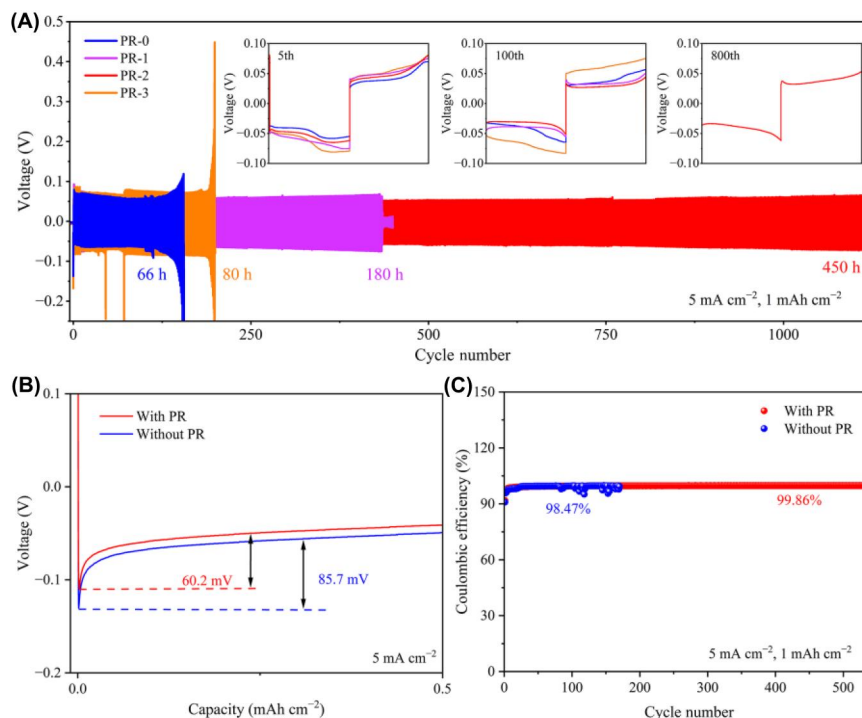


FIGURE 4 (A) Galvanostatic zinc stripping/plating of symmetric cells using different electrolytes and voltage profiles in the 5th, 100th, and 800th cycle; (B) initial zinc nucleation overpotential; and (C) CE of asymmetric cells in the electrolyte without or with PR. CE, coulombic efficiency; PR, Procion Red MX-5b.

(CE, 99.86%) in the compound electrolyte (Figure 4C). Meanwhile, voltage-capacity curves of different cycles in Figure S22 further confirmed the highly reversible zinc stripping/plating process at EEI.⁴³

The modification effect of PR on electrolyte was evaluated in Zn//NaV₃O₈·1.5H₂O full cells.⁴⁴ The full cells with PR electrolyte can deliver a higher specific capacity (Figure 5A) and exhibit better rate performance (Figure 5B) in comparison with pure ZnSO₄ electrolyte. The full cells using the PR electrolyte at different current densities deliver higher specific capacity, attributing to the protection of the hydrophobic molecular layer on the cathode to inhibit the micro-dissolution of the active material. Besides, the full cell with PR cycling over 200 times shows higher capacity (220 mAh g⁻¹) and CE (99.85%) at 1.0 A g⁻¹ (Figure 5C). More remarkably, the specific capacity of full cell using the pure electrolyte rapidly degrades and fails after 500 times at 4.0 A g⁻¹ (Figure 5D). In the electrolyte with PR, the cell can be operated for over 1000 times with a high-capacity retention rate of 78.9% (150 mAh g⁻¹) and CE of 99.90%. Furthermore, the capacity retention rate of full cell with PR was 95.53% after 24 h rest, which is much higher than that

using the electrolyte without PR (72.79% retention), indicating that PR can effectively inhibit side reactions and self-discharge (Figures 5E,F).

3 | CONCLUSION

In summary, a common polar dye, PR, was selected as an additive to regulate intrinsic properties of ZnSO₄ electrolyte and interface reaction of electrode/electrolyte in AZIBs. PR can coordinate with SO₄²⁻ to reconstruct the solvent sheath and strengthen the hydrogen bond network to reduce reactivity of free H₂O. Owing to the preferential adsorption effect, PR can serve as a hydrophobic molecular layer on the surface of the electrode, homogenizing the interfacial electric field and inducing uniform zinc stripping/plating, inhibiting the anode corrosion and cathode dissolution. Therefore, zinc symmetric cell using the optimized electrolyte can operate with a lower hysteresis voltage of more than 1120 cycles at 5 mA cm⁻² and Zn//NaV₃O₈·1.5H₂O full cell can deliver high capacity (average 170 mAh g⁻¹) and improve electrochemical stability and reversibility (cycling over 1000 times at 4 A g⁻¹). This

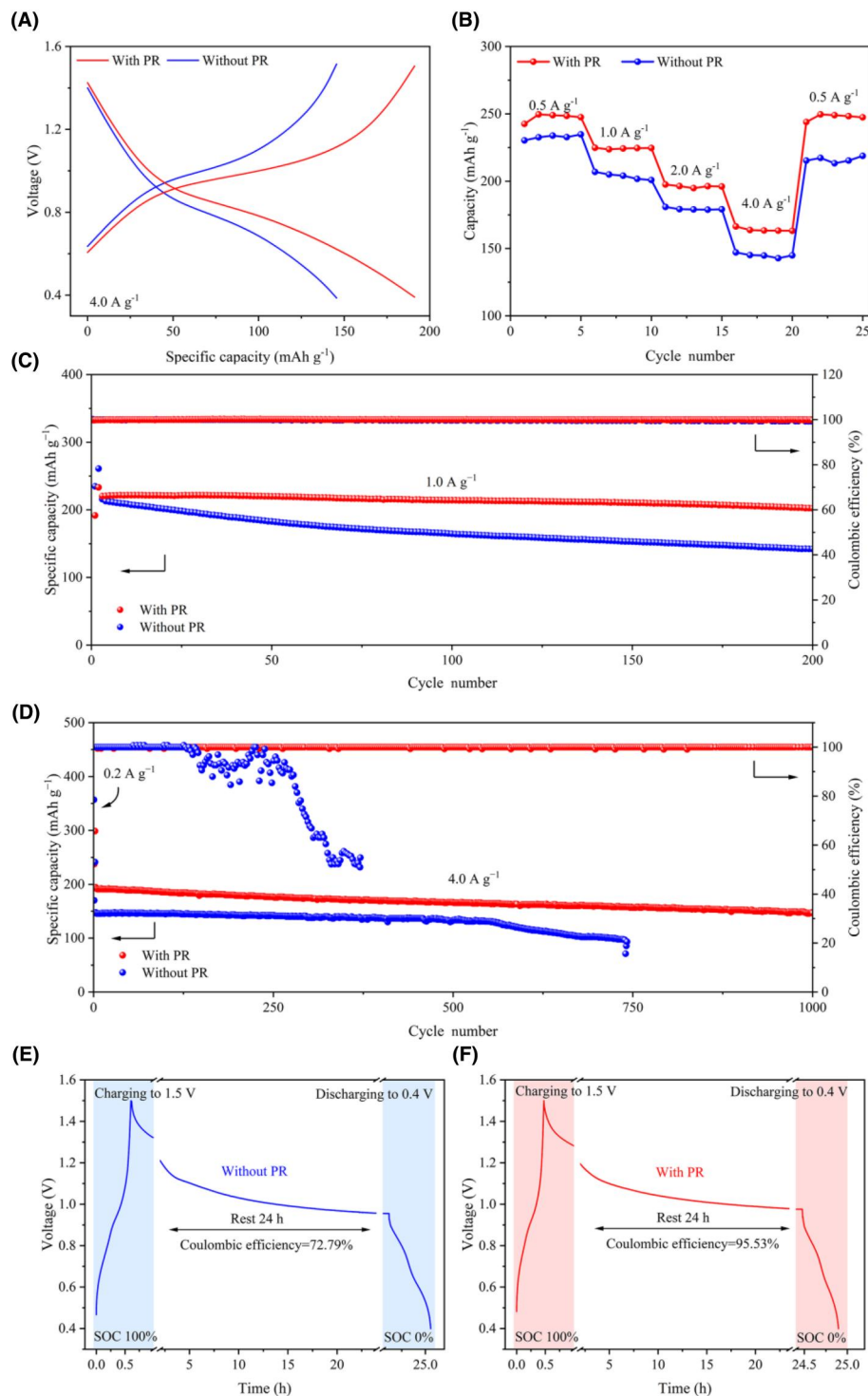


FIGURE 5 Electrochemical performance of Zn//NaV₃O₈·1.5H₂O full cells with different electrolytes. (A) Voltage-capacity profiles in the 200th cycle. (B) Rate capacities performance comparison. Cycling performance and CE at (C) 1.0 A g⁻¹ and (D) 4.0 A g⁻¹. Full cells using electrolyte (E) without and (F) with PR were first charged to 1.5 V and then rested for 24 h, followed by full discharging to 0.4 V. CE, coulombic efficiency; PR, Procion Red MX-5b; SOC, state of charge.

study may provide new thinking for additive engineering strategies to regulate the electrolyte and interfacial evolution of aqueous rechargeable zinc-ion batteries.

ACKNOWLEDGMENTS

This research was financially supported by the National Natural Science Foundation of China (No. 22109181 and No. 21975289), the Hunan Provincial

Science and Technology Plan Projects of China (No.2020JJ2042, No.2022RC3050 and No.2017TP1001), the Hunan Provincial Natural Science Foundation of China (No.2022JJ40576), and the Fundamental Research Funds for the Central Universities Central South University (2023ZZTS0511).

CONFLICT OF INTEREST STATEMENT

The authors declare no conflict of interest.

DATA AVAILABILITY STATEMENT

Research data are not shared.

ORCID

Haiyan Wang  <https://orcid.org/0000-0003-4987-6006>

REFERENCES

- Li H, Ma L, Han C, et al. Advanced rechargeable zinc-based batteries: recent progress and future perspectives. *Nano Energy*. 2019;62:550-587. <https://doi.org/10.1016/j.nanoen.2019.05.059>
- Sun D, Ye D, Liu P, et al. MoS₂/graphene nanosheets from commercial bulky MoS₂ and graphite as anode materials for high rate sodium-ion batteries. *Adv Energy Mater*. 2018; 8(10):1702383. <https://doi.org/10.1002/aenm.201702383>
- Lee B, Paek E, Mitlin D, Lee SW. Sodium metal anodes: emerging solutions to dendrite growth. *Chem Rev*. 2019;119(8): 5416-5460. <https://doi.org/10.1021/acs.chemrev.8b00642>
- Zhang Q, Yang Z, Ji H, et al. Issues and rational design of aqueous electrolyte for Zn-ion batteries. *SusMat*. 2021;1(3): 432-447. <https://doi.org/10.1002/sus2.20>
- Qin Y, Liu P, Zhang Q, et al. Advanced filter membrane separator for aqueous zinc-ion batteries. *Small*. 2020;16(39): 2003106. <https://doi.org/10.1002/smll.202003106>
- Xie C, Yang Z, Zhang Q, et al. Designing zinc deposition substrate with fully preferred orientation to elude the interfacial inhomogeneous dendrite growth. *Research*. 2022;2022: 9841343. <https://doi.org/10.34133/2022/9841343>
- Zhang Q, Luan J, Huang X, et al. Simultaneously regulating the ion distribution and electric field to achieve dendrite-free Zn anode. *Small*. 2020;16(35):2000929. <https://doi.org/10.1002/smll.202000929>
- Xie C, Ji H, Zhang Q, et al. High-index zinc facet exposure induced by preferentially orientated substrate for dendrite-free zinc anode. *Adv Energy Mater*. 2023;13(3):2203203. <https://doi.org/10.1002/aenm.202203203>
- Xie C, Liu S, Yang Z, et al. Discovering the intrinsic causes of dendrite formation in zinc metal anodes: lattice defects and residual stress. *Angew Chem Int Ed*. 2023;62(16):e202218612. <https://doi.org/10.1002/anie.202218612>
- Li W, Zhang Q, Yang Z, et al. Isotropic amorphous protective layer with uniform interfacial Zincophilicity for stable zinc anode. *Small*. 2022;18(52):2205667. <https://doi.org/10.1002/smll.202205667>
- Li R, Du Y, Li Y, et al. Alloying strategy for high-performance zinc metal anodes. *ACS Energy Lett*. 2023;8(1):457-476. <https://doi.org/10.1021/acsenenergylett.2c01960>
- Wang M, Meng Y, Li K, et al. Toward dendrite-free and anti-corrosion Zn anodes by regulating a bismuth-based energizer. *eScience*. 2022;2(5):509-517. <https://doi.org/10.1016/j.esci.2022.04.003>
- Yang Z, Li W, Zhang Q, et al. A piece of common cellulose paper but with outstanding functions for advanced aqueous zinc-ion batteries. *Mater Today Energy*. 2022;28:101076. <https://doi.org/10.1016/j.mtener.2022.101076>
- Hu Y, Zhang Y, Zhu J, Niu Z. Rational design of continuous gradient composite films for high-performance zinc-ion batteries. *Energy Stor Mater*. 2022;51:382-390. <https://doi.org/10.1016/j.ensm.2022.06.027>
- Guo S, Qin L, Zhang T, et al. Fundamentals and perspectives of electrolyte additives for aqueous zinc-ion batteries. *Energy Stor Mater*. 2021;34:545-562. <https://doi.org/10.1016/j.ensm.2020.10.019>
- Chen M, Xie S, Zhao X, et al. Aqueous zinc-ion batteries at extreme temperature: mechanisms, challenges, and strategies. *Energy Stor Mater*. 2022;51:683-718. <https://doi.org/10.1016/j.ensm.2022.06.052>
- Hao J, Yuan L, Ye C, et al. Boosting zinc electrode reversibility in aqueous electrolytes by using low-cost antisolvents. *Angew Chem Int Ed*. 2021;60(13):7366-7375. <https://doi.org/10.1002/anie.202016531>
- Sun P, Ma L, Zhou W, et al. Simultaneous regulation on solvation shell and electrode interface for dendrite-free Zn ion batteries achieved by a low-cost glucose additive. *Angew Chem Int Ed*. 2021;60(33):18247-18255. <https://doi.org/10.1002/anie.202105756>
- Cao L, Li D, Hu E, et al. Solvation structure design for aqueous Zn metal batteries. *J Am Chem Soc*. 2020;142(51):21404-21409. <https://doi.org/10.1021/jacs.0c09794>
- Wang D, Lv D, Liu H, et al. In-situ formation of nitrogen-rich solid electrolyte interphase and simultaneous regulating solvation structures for advanced Zn metal batteries. *Angew Chem Int Ed*. 2022;134(52):e202212839. <https://doi.org/10.1002/anie.202212839>
- Zhang Q, Luan J, Fu L, et al. The three-dimensional dendrite-free zinc anode on a copper mesh with a zinc-oriented polyacrylamide electrolyte additive. *Angew Chem Int Ed*. 2019; 58(44):15841-15847. <https://doi.org/10.1002/anie.201907830>
- Qin H, Kuang W, Hu N, et al. Building metal-molecule interface towards stable and reversible Zn metal anodes for aqueous rechargeable zinc batteries. *Adv Funct Mater*. 2022;32(47): 2206695. <https://doi.org/10.1002/adfm.202206695>
- Meng Q, Zhao R, Cao P, et al. Stabilization of Zn anode via a multifunctional cysteine additive. *Chem Eng J*. 2022;447: 137471. <https://doi.org/10.1016/j.cej.2022.137471>
- Ding F, Xu W, Graff GL, et al. Dendrite-free lithium deposition via self-healing electrostatic shield mechanism. *J Am Chem Soc*. 2013;135(11):4450-4456. <https://doi.org/10.1021/ja312241y>
- Li Y, Wu P, Zhong W, et al. A progressive nucleation mechanism enables stable zinc stripping-plating behavior. *Energy Environ Sci*. 2021;14(10):5563-5571. <https://doi.org/10.1039/d1ee01861b>
- Zhao R, Wang H, Du H, et al. Lanthanum nitrate as aqueous electrolyte additive for favourable zinc metal electrodeposition. *Nat Commun*. 2022;13(1):3252. <https://doi.org/10.1038/s41467-022-30939-8>
- Yan C, Li H-R, Chen X, et al. Regulating the inner Helmholtz plane for stable solid electrolyte interphase on lithium metal anodes. *J Am Chem Soc*. 2019;141(23):9422-9429. <https://doi.org/10.1021/jacs.9b05029>
- Borodin O, Ren X, Vatamanu J, von Wald Cresce A, Knap J, Xu K. Modeling insight into battery electrolyte electrochemical stability and interfacial structure. *Acc Chem Res*. 2017;50(12): 2886-2894. <https://doi.org/10.1021/acs.accounts.7b00486>
- Bard AJ, Faulkner LR. *Electrochemical Methods: Fundamentals and Applications*. 2nd ed. Wiley; 2001.
- Balos V, Imoto S, Netz RR, et al. Macroscopic conductivity of aqueous electrolyte solutions scales with ultrafast microscopic ion motions. *Nat Commun*. 2020;11(1):1611. <https://doi.org/10.1038/s41467-020-15450-2>

31. Wang M, Ma J, Meng Y, et al. High-capacity zinc anode with 96% utilization rate enabled by solvation structure design. *Angew Chem Int Ed.* 2022;135(3):e202214966. <https://doi.org/10.1002/ange.202214966>
32. Liu J, Wang Y, Liu F, Cheng F, Chen J. Improving metallic lithium anode with NaPF₆ additive in LiPF₆-carbonate electrolyte. *J Energy Chem.* 2020;42:1-4. <https://doi.org/10.1016/j.jchem.2019.05.017>
33. Zu X, Zhang L, Qian Y, Zhang C, Yu G. Molecular engineering of azobenzene-based anolytes towards high-capacity aqueous redox flow batteries. *Angew Chem Int Ed.* 2020;132(49):22347-22354. <https://doi.org/10.1002/ange.202009279>
34. Zhang Q, Xia K, Ma Y, et al. Chaotropic anion and fast-kinetics cathode enabling low-temperature aqueous Zn batteries. *ACS Energy Lett.* 2021;6(8):2704-2712. <https://doi.org/10.1021/acseenergylett.1c01054>
35. Li TC, Lim Y, Li XL, et al. A universal additive strategy to reshape electrolyte solvation structure toward reversible Zn storage. *Adv Energy Mater.* 2022;12(15):2103231. <https://doi.org/10.1002/aenm.202103231>
36. Yang Z, Zhang Q, Xie C, et al. Electrochemical interface reconstruction to eliminate surface heterogeneity for dendrite-free zinc anodes. *Energy Stor Mater.* 2022;47:319-326. <https://doi.org/10.1016/j.ensm.2022.02.022>
37. Zhang W, Lu Y, Wan L, et al. Engineering a passivating electric double layer for high performance lithium metal batteries. *Nat Commun.* 2022;13(1):2029. <https://doi.org/10.1038/s41467-022-29761-z>
38. Zhao F, Jing Z, Guo X, et al. Trace amounts of fluorinated surfactant additives enable high performance zinc-ion batteries. *Energy Stor Mater.* 2022;53:638-645. <https://doi.org/10.1016/j.ensm.2022.10.001>
39. Mao J, Iocozzia J, Huang J, Meng K, Lai Y, Lin Z. Graphene aerogels for efficient energy storage and conversion. *Energy Environ Sci.* 2018;11(4):772-799. <https://doi.org/10.1039/c7ee03031b>
40. Kao C-C, Ye C, Hao J, Shan J, Li H, Qiao S-Z. Suppressing hydrogen evolution via anticatalytic interfaces toward highly efficient aqueous Zn-ion batteries. *ACS Nano.* 2023;17(4):3948-3957. <https://doi.org/10.1021/acsnano.2c12587>
41. Zhou J, Wu F, Mei Y, et al. Establishing thermal infusion method for stable zinc metal anodes in aqueous zinc-ion batteries. *Adv Mater.* 2022;34(21):2200782. <https://doi.org/10.1002/adma.202200782>
42. Zhang Q, Luan J, Tang Y, Ji X, Wang H. Interfacial design of dendrite-free zinc anodes for aqueous zinc-ion batteries. *Angew Chem Int Ed.* 2020;59(32):13180-13191. <https://doi.org/10.1002/anie.202000162>
43. Qi K, Zhu W, Zhang X, et al. Enamel-like layer of nano-hydroxyapatite stabilizes Zn metal anodes by ion exchange adsorption and electrolyte pH regulation. *ACS Nano.* 2022;16(6):9461-9471. <https://doi.org/10.1021/acsnano.2c02448>
44. Wan F, Zhang L, Dai X, Wang X, Niu Z, Chen J. Aqueous rechargeable zinc/sodium vanadate batteries with enhanced performance from simultaneous insertion of dual carriers. *Nat Commun.* 2018;9(1):1656. <https://doi.org/10.1038/s41467-018-04060-8>

SUPPORTING INFORMATION

Additional supporting information can be found online in the Supporting Information section at the end of this article.

How to cite this article: Wang H, Hu C, Yang Z, et al. A common polar dye additive as corrosion inhibitor and leveling agent for stable aqueous zinc-ion batteries. *Electron.* 2024;2(1):e21. <https://doi.org/10.1002/elt2.21>